The Stefan Problem with Internal Heat Generation in Cylindrical Coordinates

Lyudmyla Barannyk
Department of Mathematics
University of Idaho
Moscow, Idaho 83843
Email: barannyk@uidaho.edu

John C. Crepeau*
Department of Mechanical Engineering
University of Idaho
Moscow, Idaho 83843
Email: crepeau@uidaho.edu

Patrick Paulus
Department of Mechanical Engineering
University of Idaho
Moscow, Idaho 83843
Email: paul2217@vandals.uidaho.edu

Alexey Sakhnov
Kutateladze Institute of Thermophysics SB RAS
Novosibirsk, 630090, Russia
Email: aleksei_sakhnov@mail.ru

Sidney D.V. Williams
Student, Student Member of ASME
Department of Physics
Georgia Institute of Technology
Atlanta, Georgia 30332
Email: swilliams425@gatech.edu

We study the evolution of the solid-liquid interface during melting and solidification of a material with constant internal heat generation with prescribed temperature conditions at the boundary of a cylinder. The movement of the interface is assumed to be slow enough that the heat equations in both phases can be solved by splitting them into transient and quasi steady-state components which can then be treated through separation of variables (referred to as a weakly time dependent approximation). This results in a nonlinear, first-order ordinary differential equation that involves infinite Bessel series terms. The initial value problem is solved numerically, and solutions are compared to the method of catching of the front into a space grid node which does not rely on the weakly time dependent approximation, and the enthalpy-porosity method built into ANSYS-Fluent which accounts for the formation of a mushy zone.

The weakly time dependent approximation agrees very well with the method of catching of the front into a space grid node, with noticeable differences only appearing at large values of Stefan number, and at early times. Therefore, the weakly time dependent approximation is valid for most configurations of the system. The sharp-interface model presented in this paper contains exponentially decaying terms in the form of infinite Bessel series for the temperature gradients in both the solid and liquid phases. The agreement between the ANSYS-Fluent simulation and the weakly time dependent approximation is excellent. Noticeable difference only occurs at large Stefan numbers, and only at early times. This implies that neglecting the mushy zone is valid for most configurations of the system. At higher Stefan numbers, the system approaches steady-state faster than for lower Stefan numbers. For both melting and solidification, the temperature equilibrates to a parabolic profile.

Nomenclature

A_n, B_n Bessel Series Coefficients
c_1, c_2, c_3, c_4 Integration Constants
f,g Separation of Variables Functions
Δh_f Heat of Fusion
J_0, Y_0 Bessel Functions of the First and Second Kind
k Thermal Conductivity
$\dot{q}$ Internal Heat Generation
$\dot{Q}$ Nondimensional Heat Generation
r Radial Direction
r_0 Distance to the Centerline
s Distance to the Phase Change Front
St Stefan Number
t Time
T Temperature
T_0 Temperature Along the Surface of the Cylinder
T_m Phase Change Temperature
z_0 Zeros of the Bessel Function
α Thermal Diffusivity
ϕ, Φ Initial Temperature Profiles
η Nondimensional Distance
λ, $\tilde{\lambda}$ Eigenvalues
θ Nondimensional Temperature
ρ Density
τ Nondimensional Time
ζ Nondimensional Distance to the Phase Change Front
liq Liquid
sol Solid

*Corresponding Author

1 Introduction

The classical solid-liquid phase change problem has been studied for over one hundred years, first by Lamé and Clapeyron [1], then independently by Stefan [2] whose name is now synonymous with this class of problems [3]. Stefan problems remain an active area of research today [4-6]. While the classical problem has been well analyzed, a subset of the problem, namely phase change driven by internal heat generation, has been very sparsely explored. Various techniques have been used to study phase change driven by internal heat generation including, perturbation analysis [7] and lumped parameter techniques [8]. Applications of phase change with internal heat generation include geological heat transfer [9-10] and nano-enhanced phase change materials [11] as well as nuclear safety analysis[12]. Chen et al. [13] used a simple transient conduction model to determine when a nuclear fuel pin began to melt. El-Genk and Cronenberg [14] studied the effects of internal heat generation on transient freezing in a reactor shield plug using a successive approximation technique. Cheung et al. [15] studied melting and freezing in a heat generating slab between two semi-infinite walls. Chan et al. [16] modeled phase change in semi-transparent materials induced by radiation heat transfer. Chan and Hsu [17] applied the enthalpy method to study the formation of the mushy zone in problems with internal heat generation. Le Tellier, et al. [18] used three different techniques to study the Stefan problem and included the effects of convection in the liquid phase to study the boundary heat flux closure relations. Tang, et al. [19] numerically studied melting processes in a nuclear fuel rod using the half-boundary method applied to an enthalpy formulation. In addition to the melting problem, Dubey and Sharma [20] also modelled the multi-phase flow of nuclear fuel in a fast reactor fuel rod. An and Su [21] used finite difference techniques to study the melting processes in a nuclear fuel rod.

In a finite domain, the Stefan problem no longer yields to similarity solution. Therefore, it must be solved by approximation. Changing the Stefan number modulates the speed of the interface, therefore, it would make sense to use an approximation dependent on the time derivative of the interface location. In classical electrodynamics, it is common to adopt a "quasi-static" approximation. Such an approximation allows the application of electrostatic equations to electrodynamic systems, the limitation being that the charge and current densities cannot be varying quickly in time. We can adapt this to the Stefan problem by introducing the *weakly time dependent interface approximation* which, providing the interface is not moving too quickly, allows the heat equation to be solved as if the interface is simply a static boundary. With this treatment, the cylindrical non-homogenous heat equation is a linear partial differential equation which can be treated by separation of variables.

In previous works [28,29], the behavior of the interface between the liquid and solid phases have been explored in cylindrical geometry with the assumption that there is a sharp interface. In actual melting phenomena, an intermediate phase forms that is neither pure liquid, nor pure solid, this phase has been named the "mushy zone" (cite something here). This is most commonly modelled through Voller and Prakesh's enthalpy-porosity method [34], which is implemented into the ANSYS FLUENT software (cite Fluent theory manual). In the current work, we focus on solving the finite Stefan problem in cylindrical coordinates with fixed temperature at the outer boundary and sharp interface assumption approximately. The results can then be compared to the enthalpy-porosity method to test the validity of the sharp interface approximation.

2 Solution Derivation

The goal of this project was to solve the Stefan problem (solid-liquid phase change) in cylindrical coordinates, where the phase change is driven by internal heat generation of the material. The following assumptions are considered in this analysis: (1) the internal heat generation and the thermophysical properties of the materials are equal and constant in both the solid and liquid phases; (2) the material changes phase at only a single temperature, T_m; (3) we neglect the formation of the mushy zone so that there is a single, distinct interface between the phases; (4) there is no temperature variation circumferentially in the cylinder so that heat transfers solely in the radial direction; finally, (5) all forms of convection are assumed negligible. This last assumption is justified in Appendix A. A schematic of the system's geometry is given in Fig.1.

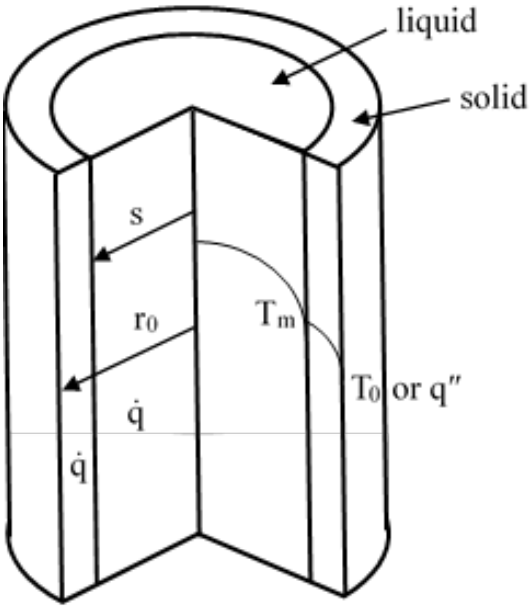

Fig. 1: Schematic diagram of the phase change problem in a cylindrical geometry

Energy transfer is governed by the heat equation with internal heat generation in cylindrical coordinates, and is given

by [30], which neglects convection

$$\frac{1}{r}\frac{\partial}{\partial r}\left(r\frac{\partial T}{\partial r}\right)+\frac{\dot{q}}{k}=\frac{1}{\alpha}\frac{\partial T}{\partial t} \qquad T=T(r,t),\ \ 0\le s\le r_0,\ \ 0\le t\le\infty \tag{1}$$

Along the interface between the solid and liquid phases, an energy balance yields [31],

$$k_{liq}\frac{\partial T_{liq}(r,t)}{\partial r}\bigg|_{r=s(t)}+\rho_{sol}\Delta h_f\frac{ds(t)}{dt}=k_{sol}\frac{\partial T_{sol}(r,t)}{\partial r}\bigg|_{r=s(t)} \tag{2}$$

With constant surface temperature boundary conditions, the temperature at the surface is T_0. The temperature profiles in the liquid and solid phases will be determined, then inserted into the interface equation, Eq.(2).

In the liquid phase, the boundary conditions and initial condition are,

$$\frac{\partial T_{liq}(r,t)}{\partial r}\bigg|_{r=0}=0 \qquad T_{liq}(s(t),t)=T_m \qquad T_{liq}(r,0)=\phi_{liq} \tag{3}$$

In the solid phase the boundary conditions and initial condition are,

$$T_{sol}(s(t),t)=T_m \qquad T_{sol}(r_0,t)=T_0 \qquad T_{sol}(r,0)=\phi_{sol}(r) \tag{4}$$

Following the assumption that the thermophysical properties are equal in both phases, the subscripts for those terms will be dropped. We then nondimensionalize the variables in the following fashion:

$$\eta=\frac{r}{r_0},\ \ \tau=\frac{\alpha t}{r_0^2},\ \ \theta(\eta,\tau)=\frac{T(r,t)-T_0}{T_m-T_0},\ \ \zeta=\frac{s(t)}{r_0} \qquad St=\frac{c_p(T_m-T_0)}{\Delta h_f},\ \ \dot{Q}=\frac{\dot{q}r_0^2}{k(T_m-T_0)} \tag{5}$$

Introducing these into the heat equation (Eq.(1)) and boundary conditions (Eq.(3) and Eq.(4)) yields,

$$\frac{1}{\eta}\frac{\partial}{\partial\eta}\left(\eta\frac{\partial\theta}{\partial\eta}\right)+\dot{Q}=\frac{\partial\theta}{\partial\tau} \tag{6}$$

with the nondimensional boundary conditions given in the liquid and solid regions respectively, by,

$$\frac{\partial\theta_{liq}(0,\tau)}{\partial\eta}=0,\ \theta_{liq}(\zeta(\tau),\tau)=1,\ \theta_{liq}(\eta,0)=\Phi_{liq}(\eta) \tag{7}$$

$$\theta_{sol}(\zeta(\tau),\tau)=1,\ \theta_{sol}(1,\tau),\ \theta_{sol}(\eta,0)=\Phi_{sol}(\eta) \tag{8}$$

where Φ represents the initial temperature profile. The interface equation becomes,

$$\frac{\partial\theta_{liq}}{\partial\eta}\bigg|_{\eta=\zeta(\tau)}+\frac{1}{St}\frac{d\zeta}{d\tau}=\frac{\partial\theta_{sol}}{\partial\eta}\bigg|_{\eta=\zeta(\tau)} \tag{9}$$

In order to solve the heat equation defined above(Eq.(6)), we must deal with the variable boundary location inherent in this problem. We accomplish this by defining a weakly time dependent approximation, stating that the interface is only weakly time dependent and thus, for the purpose of separating variables, can be treated as a location static in time. Equations (6)-(9) provide a definition of the problem to be solved. To find the solution, we first separate the liquid temperature profile into transient and quasi steady-state components, [32]

$$\theta_{liq}(\eta,\tau)=\theta_{liq,tr}(\eta,\tau)+\theta_{liq,ss}(\eta) \qquad 0<\eta<\zeta(\tau) \tag{10}$$

"Quasi" denotes that the "steady-state" component of the solution depends on the interface, and thus implicitly on time. However, by making the weakly time dependent approximation, we can treat the steady-state as fully steady-state, for the purposes of solving the heat equation. Substituting the separated temperature profile into Equation (6) yields,

$$\frac{1}{\eta}\frac{\partial}{\partial\eta}\left(\eta\frac{\partial\theta_{liq,tr}}{\partial\eta}\right)+\frac{1}{\eta}\frac{\partial}{\partial\eta}\left(\eta\frac{\partial\theta_{liq,ss}}{\partial\eta}\right)+\dot{Q}=\frac{\partial\theta_{liq,tr}}{\partial\tau} \tag{11}$$

We then substitute Equation (10) into the boundary and initial conditions (Eq.(7)) to get,

$$\frac{\partial\theta_{liq,tr}(0,\tau)}{\partial\eta}+\frac{\partial\theta_{liq,ss}(0)}{\partial\eta}=0, \qquad \theta_{liq,tr}(\zeta(\tau),\tau)+\theta_{liq,ss}(\zeta(\tau),\tau)=1, \qquad \theta_{liq,tr}(\eta,0)+\theta_{liq,ss}(\eta)=\Phi_{liq}(\eta) \tag{12}$$

Using the principle of superposition, Eq.(11) can be separated into transient and quasi steady-state portions. We find for the transient part,

$$\frac{1}{\eta}\frac{\partial}{\partial\eta}\left(\eta\frac{\partial\theta_{liq,tr}}{\partial\eta}\right)+\dot{Q}=\frac{\partial\theta_{liq,tr}}{\partial\tau} \tag{13}$$

with the boundary and initial conditions,

$$\frac{\partial\theta_{liq,tr}(0,\tau)}{\partial\eta}=0,\ \ \theta_{liq,tr}(\zeta(\tau),\tau)=0 \qquad \theta_{liq,tr}(\eta,0)=\Phi_{liq}(\eta)-\theta_{liq,ss}(\eta) \tag{14}$$

The quasi steady-state portion becomes,

$$\frac{1}{\eta}\frac{d}{d\eta}\left(r\frac{d\theta_{liq,ss}}{d\eta}\right) = -\dot{Q} \tag{15}$$

with boundary conditions,

$$\frac{d\theta_{liq,ss}(0)}{d\eta} = 0, \;\; \theta_{liq,ss}(\zeta(\tau)) = 1 \tag{16}$$

Solving the quasi steady-state problem first, we integrate Eq.(15) twice and apply the boundary conditions of Eq.(16) to find,

$$\theta_{liq,ss}(\eta) = \frac{1}{4}\dot{Q}(\zeta^2 - \eta^2) + 1 \tag{17}$$

For the transient portion of the liquid phase, we assume a solution to Equation (13) as the product of two functions dependent only on η and τ respectively, again, we can do this as long as the time dependence of the interfaces is assumed very weak,

$$\theta_{liq,tr}(\eta,\tau) = f(\eta)g(\tau) \tag{18}$$

Using the method of separation of variables [33] we find,

$$\begin{aligned} f(\eta) &= c_1 J_0(\lambda\eta) + c_2 Y_0(\lambda\eta) \\ g(\tau) &= e^{-\lambda^2\tau} \end{aligned} \tag{19}$$

Where J_0 and Y_0 are Bessel functions of the first and second kind, respectively. The function $f(\eta)$ is bounded at $\eta = 0$ so $c_2 = 0$ because $Y_0(\lambda\eta) \to \infty$ as $\eta \to 0^+$. Applying the boundary condition $f(\eta = 0) = 0$ (from Equation (14)), we get,

$$f(\zeta) = c_1 J_0(\lambda\eta) = 0 \tag{20}$$

To obtain a nontrivial solution, i.e., $c_1 \neq 0$ the following condition must hold,

$$J_0(\lambda\zeta(\tau)) = 0 \tag{21}$$

Denoting the zeroes of the Bessel function as z_{0n}, the eigenvalues become

$$\lambda_n = \frac{z_{0n}}{\zeta(\tau)} \tag{22}$$

The associated eigenfunctions are $J_0(\lambda_n\eta)$ that are orthogonal $[0,\zeta]$ with weight η, as dictated by Sturm-Liouville theory.

The nondimensional temperature profile in the liquid phase is then,

$$\theta_{liq,tr}(\eta,\tau) = \sum_{n=1}^{\infty} A_n e^{-\lambda_n^2\tau} J_0(\lambda_n\eta) \tag{23}$$

To solve for the coefficients A_n, we apply the initial conditions given in Equation (14),

$$\theta_{liq,tr}(\eta,0) = \Phi_{liq}(\eta) - \theta_{liq,ss} = \sum_{n=1}^{\infty} A_n J_0(\lambda_n\eta) \tag{24}$$

By multiplying both sides of Eq.(24) by $J_0(\lambda_n\eta)\eta$ and integrating from 0 to $\zeta(\tau)$, and using orthogonality of of the eigenfunctions, we can show that,

$$A_n = \frac{\int_0^{\zeta(\tau)} (\Phi_{liq} - \theta_{liq,ss}) J_0(\lambda_n\eta)\eta d\eta}{\frac{1}{2}\zeta^2(\tau) J_1^2(\lambda_n\eta)} \tag{25}$$

Therefore, the complete temperature profile in the liquid phase becomes,

$$\theta_{liq}(\eta,\tau) = \sum_{n=1}^{\infty} A_n e^{-\lambda_n^2\tau} J_0(\lambda_n\eta) + \frac{1}{4}\dot{Q}(\zeta^2 - \eta^2) + 1 \tag{26}$$

With A_n and λ_n defined in (25) and (22), respectively. The initial conditions will be discussed later.

A similar process holds for the solid phase. The temperature profile in the solid is separated into transient and quasi steady-state profiles,

$$\begin{aligned} \theta_{sol}(\eta,\tau) &= \theta_{sol,tr}(\eta,\tau) + \theta_{sol,ss}(\eta) \\ \zeta(tau) &< \eta < 1 \end{aligned} \tag{27}$$

Substituting into the heat diffusion equation (6) yields,

$$\frac{1}{\eta}\frac{\partial}{\partial\eta}\left(\eta\frac{\partial\theta_{sol,tr}}{\partial\eta}\right) + \frac{1}{\eta}\frac{\partial}{\partial\eta}\left(\eta\frac{\partial\theta_{sol,ss}}{\partial\eta}\right) + \dot{Q} = \frac{\partial\theta_{sol,tr}}{\partial\tau} \tag{28}$$

After separating the quasi steady-state and transient parts, we solve the quasi steady-state portion first. For Eq.(28) this becomes,

$$\frac{1}{\eta}\frac{d}{d\eta}\left(r\frac{d\theta_{sol,ss}}{d\eta}\right) = -\dot{Q} \tag{29}$$

with boundary conditions,

$$\theta_{sol,ss}(\zeta(\tau)) = 1, \;\; \theta_{sol,ss}(1) = 0 \tag{30}$$

By integrating twice and applying the boundary conditions we find,

$$\theta_{sol,ss}(\eta) = \frac{1}{4}\dot{Q}(1-\eta^2) + \left(\frac{1}{4}\dot{Q}(\zeta(\tau)-1)+1\right)\frac{\ln\eta}{\ln\zeta(\tau)} \tag{31}$$

The transient portion of Eq.(27) is,

$$\frac{1}{\eta}\frac{\partial}{\partial\eta}\left(\eta\frac{\partial\theta_{sol,tr}}{\partial\eta}\right) + \dot{Q} = \frac{\partial\theta_{sol,tr}}{\partial\tau} \tag{32}$$

with the boundary and initial conditions,

$$\begin{aligned} \frac{\partial\theta_{sol,tr}(0,\tau)}{\partial\eta} = 0, \quad \theta_{liq,tr}(\zeta(\tau),\tau) = 0 \\ \theta_{sol,tr}(\eta,0) = \Phi_{liq}(\eta) - \theta_{liq,ss}(\eta) \end{aligned} \tag{33}$$

As in the solution for the liquid phase, we use separation of variables to solve the initial value boundary problem as defined in Eqns (32) and (33), to find,

$$\begin{aligned} f(\eta) = c_3 J_0(\lambda\eta) + c_4 Y_0(\lambda\eta) \\ g(\tau) = e^{-\lambda^2\tau} \end{aligned} \tag{34}$$

Applying the boundary conditions $f(\zeta(\tau)) = 0$, $f(1) = 0$ to the $f(\eta)$ relation in Eq.(34) we find,

$$\begin{aligned} 0 = c_3 J_0(\lambda\zeta(\tau)) + c_4 Y_0(\lambda\zeta(\tau)) \\ 0 = c_3 J_0(\lambda) + c_4 Y_0(\lambda) \end{aligned} \tag{35}$$

The values of $c_3 = c_4 = 0$ lead to the trivial solution. For a non-trivial solution, the following determinant must hold,

$$\begin{vmatrix} J_0(\lambda\zeta(\tau)) & Y_0(\lambda\zeta(\tau)) \\ J_0(\lambda) & Y_0(\lambda) \end{vmatrix} = 0 \tag{36}$$

or,

$$J_0(\lambda\zeta(\tau))Y_0(\lambda) - Y_0(\lambda\zeta(\tau))J_0(\lambda) = 0 \tag{37}$$

The zeroes of Eq.(37) are eigenvalues, which are denoted by $\tilde{\lambda}_n$. These zeroes are computed numerically using Newton's root finding method and the asymptotic behavior of Bessel functions. We apply the boundary condition $f(1) = 0$ to obtain,

$$f(1) = 0 = c_3 J_0(\lambda) + c_4 Y_0(\lambda) \tag{38}$$

by rearranging we obtain

$$c_3 = -c_4\frac{Y_0(\lambda))}{J_0(\lambda)} \tag{39}$$

Substituting this back into (34) yields

$$f_n(\eta) = Y_0(\tilde{\lambda}_n\eta) - \frac{Y_0(\tilde{\lambda}_n)}{J_0(\tilde{\lambda}_n)}J_0(\tilde{\lambda}_n) \tag{40}$$

The differential equation for which $f_n(\eta)$ is a solution is a Sturm-Liouville boundary value problem on $[\zeta, 1]$.(Cite Haberman)

Multiplying Eq.(40) by the time relation in Eq.(34) and summing over all n gives the transient solution,

$$\theta_{tr,sol}(\eta,\tau) = \sum_{n=1}^{\infty} B_n f_n(\eta) e^{\tilde{\lambda}_n^2\tau} \tag{41}$$

The coefficients B_n can be solved for by applying the initial condition in Eq.(33),

$$\theta_{tr,sol}(\eta,0) = \Phi_{sol}(\eta) - \theta_{ss,sol}(\eta) = \sum_{n=1}^{\infty} B_n f_n(\eta) \tag{42}$$

From the orthogonality [33] of the eigenfunctions f_n, we multiply both sides by $f_m(\eta)\eta$ then integrate from $\zeta(\tau)$ to 1 to obtain,

$$B_n = \frac{\int_{\zeta(\tau)}^1 (\Phi_{sol}(\eta) - \theta_{ss,sol}(\eta)) f_n(\eta)\eta d\eta}{\int_{\zeta(\tau)}^1 f_n^2(\eta)\eta d\eta} \tag{43}$$

Therefore, the temperature distribution in the solid is given by,

$$\begin{aligned} \theta_{sol}(\eta,\tau) = \sum_{n=1}^{\infty} B_n f_n(\eta) e^{\tilde{\lambda}_n^2\tau} + \frac{1}{4}\dot{Q}(1-\eta^2) \\ + \left(\frac{1}{4}\dot{Q}(\zeta(\tau)-1)+1\right)\frac{\ln\eta}{\ln\zeta(\tau)} \end{aligned} \tag{44}$$

with $f_n(\eta)$ and B_n being defined in Eqns. (40) and (43), respectively. The values of $\tilde{\lambda}_n$ are the roots of Eq.(**??**). Equations (26) and (44) give approximate temperature profiles in the liquid and solid phases, respectively. From those relations, the temperature gradients can be calculated and evaluated at $\eta = \zeta(\tau)$ (the location of the solid-liquid interface), then inserted into the interface equation (Eq.(9)).

From the temperature profile in the liquid phase, Eq.(26), we can determine the temperature gradient to be,

$$\left.\frac{\partial\theta_{liq}}{\partial\eta}\right|_{\eta=\zeta(\tau)} = -\sum_{n=1}^{\infty}\lambda_n A_n J_1(\lambda_n\zeta(\tau)) e^{-\lambda_n^2\tau} - \frac{1}{2}\dot{Q}\zeta(\tau) \tag{45}$$

From the temperature profile in the solid phase, Eq.(44), the

temperature gradient becomes,

$$\left.\frac{\partial \theta_{sol}}{\partial \eta}\right|_{\eta=\zeta(\tau)} = -\sum_{n=1}^{\infty} \tilde{\lambda}_n B_n e^{-\tilde{\lambda}_n^2 \tau}\left[Y_1(\tilde{\lambda}_n \zeta(\tau)) - \frac{Y_0(\tilde{\lambda}_n)}{J_0(\tilde{\lambda}_n)}\right] + \left(\frac{\dot{Q}}{4}(\zeta^2(\tau)-1)+1\right)\frac{1}{\zeta(\tau)\ln\zeta(\tau)} - \frac{1}{2}\dot{Q}\zeta(\tau) \tag{46}$$

Inserting these into the nondimensional interface equation (Eq.(9)) then gives a first-order, ordinary differential equation approximately governing the motion of the interface, $\zeta(\tau)$:

$$\begin{aligned} &-\sum_{n=1}^{\infty} \lambda_n A_n J_1(\lambda_n \zeta(\tau)) e^{-\lambda_n^2 \tau} + \frac{1}{St}\frac{d\zeta(\tau)}{d\tau} \\ &= -\sum_{n=1}^{\infty} \tilde{\lambda}_n B_n e^{-\tilde{\lambda}_n^2 \tau}\left[Y_1(\tilde{\lambda}_n \zeta(\tau)) - \frac{Y_0(\tilde{\lambda}_n)}{J_0(\tilde{\lambda}_n)}\right] \\ &\quad + \left(\frac{\dot{Q}}{4}(\zeta^2(\tau)-1)+1\right)\frac{1}{\zeta(\tau)\ln\zeta(\tau)} \end{aligned} \tag{47}$$

The boundary and initial conditions for melting are,

$$\begin{aligned} \Phi_{liq}(\eta) &= 1 \\ \Phi_{sol}(\eta) &= (1-\eta^2) \\ \tau = 0, \;\; \zeta(0) &= 0 \end{aligned} \tag{48}$$

and the boundary and initial conditions for solidification are as follows:

$$\begin{aligned} \Phi_{liq}(\eta) &= \frac{\dot{Q}}{4}(1-\eta^2)+1 \\ \Phi_{sol}(\eta) &= 1 \\ \tau = 0, \;\; \zeta(0) &= 1 \end{aligned} \tag{49}$$

The initial temperature profiles are based on the parabolic profiles which are characteristic of heat transfer problems with internal heat generation.

The relation governing the movement of the solid-liquid interface, Eq.(47), along with the appropriate initial conditions (Eqns. (48) or (49)) can be evaluated numerically and compared to the quasi-static solution given in [28]. The difference between these two approximate solutions is that the weakly time dependent approximation allows for tracking of the temperature evolution over time, whereas the quasi-static solution assumes a static temperature.

3 The Method of Catching of the Front Into a Space Grid Node

The accuracy of the weakly time dependent approximation has been verified through comparison to the method of catching of the front into a space grid node which discretizes space arbitrarily, and discretizes time in steps equal to the time it takes for the moving interface to move from space node to space node. This time step can be derived from the interface equation by Taylor expanding temperature in space, and using the second derivative given by the nonhomogenous heat Equation (6) we derive the following for timestep:

$$\begin{aligned} \Delta\tau &= \frac{\frac{\Delta r^2}{2}(a+b)(\theta_m - \theta_{i-1,j}) + \frac{\Delta r}{St}}{b(\theta_{i,j+1}-\theta_m) - a(\theta_m - \theta_{i,j-1}) + \dot{Q}\frac{\Delta r^2}{2}(a+b)} \\ a &= \frac{1}{\Delta r + \frac{\Delta r^2}{2r}} \\ b &= \frac{1}{\Delta r - \frac{\Delta r^2}{2r}} \end{aligned} \tag{50}$$

For each time step, the Thomas Algorithm(cite) is used to solve for temperature at every spatial node according to (6). The results of this computation were presented in Novosibirsk during 2019 by Creapeau et. al. (Cite Russian Paper) which showed that, except for early times at large Stefan numbers, the weakly time dependent approximate solution matched the numerical simulation very closely. Fig.2 below also displays these results. Therefore, under most circumstances, the weakly time dependent solution accurately describes the system, and is a valid representative of the sharp interface model.

This method does not allow the time step to be set directly. Nevertheless, the space step can control the time step. It is worth to noting that the time step decreases with an increase of Stefan number which is equivalent to a more intensive melting process. Convergence tests were done for the space grid. At 200 nodes, the melting front distribution did not depend on the number of nodes in space grid. However, we used a space grid with 9000 nodes in order to reach the position of the interphase border in the steady-state regime.

4 Results and Discussion

With Eq.(47) derived, and verified (Fig.2), we can numerically solve the initial value problem for either melting (Eq.(48)) or solidification (Eq.(49)) and compare the results to finite volume solutions using ANSYS-Fluent software. This software uses the enthalpy-porosity method of Voller and Prakash [34] to model phase change process and includes the influence of the mushy zone.

The core difference between the Stefan formulation and the enthalpy method is that the Stefan method uses the strong form of the heat equation, while the enthalpy method uses a weak form solution to the energy equation. The strong form requires us to track or "capture" the front through secondary equations in the form of an energy balance at the interface. The weak form solution, on the other hand, allows the phase change phenomenon to occur without direct tracking. It does not require a sharp interface, or even an interface at all, and can model heat transfer even past the point of total melting or

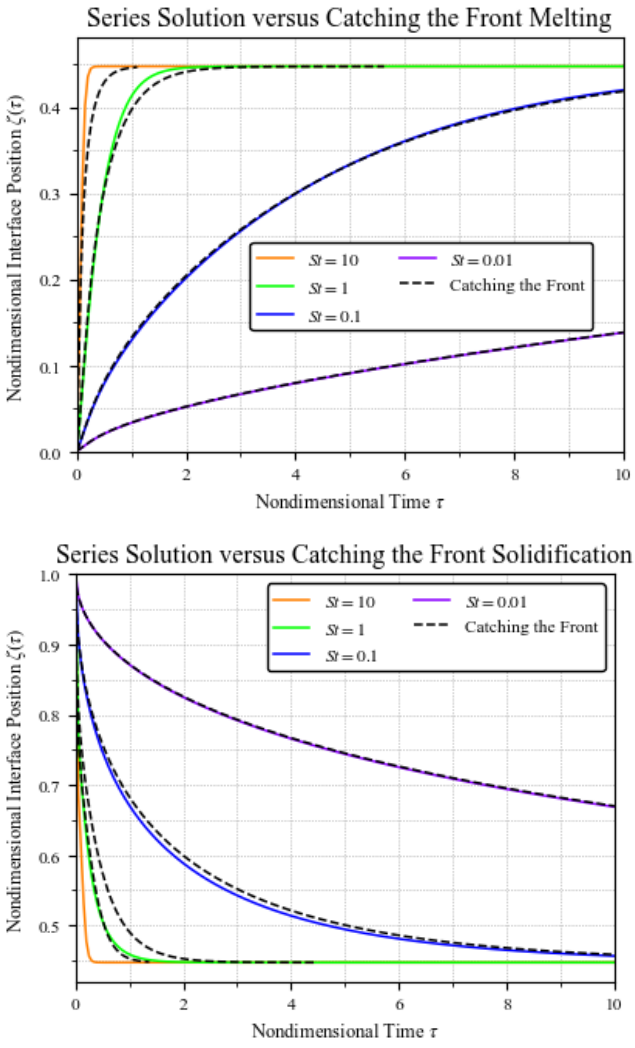

Fig. 2: A comparison between the method of catching of the front into a space grid node, and the weakly time dependent approximation for both melting and solidification with $\dot{Q} = 5$. The catching the front method curves terminate early due to the computation terminating when the steady state is reached, due to its reliance on a moving boundary for time-step calculation. Extrapolation to $\tau = 10$ was not done to make the contrast obvious.

solidification. From an implementation perspective, the difference is that the Stefan problem solutions solve for interface position, then generate temperature profiles commensurate with the interface position; whereas the enthalpy method solutions solve for the temperature and enthalpy fields, and liquid fraction is used to calculate interface position in post-processing.

Figure 3 compares the solutions of Eq.(47) with the numerical finite volume solutions during solidification for $\dot{Q} = 5$ (which was selected as the smallest integer $\dot{Q}$ which allows for interface evolution, as justified in Appendix B)and four Stefan numbers, $St = 0.01$, 0.1, 1.0 and 10.0. Lower Stefan numbers correspond to slower moving phase change fronts. At Stefan numbers of $St = 0.01$ and 0.1, the weakly time dependent solutions closely match the numerical solutions. This is expected since the phase change front moves slowly for these values of St. As the Stefan number increases, the weakly time dependent solutions diverge from the numerical solutions. This is due both to numerical diffusion, the "smoothing out" of sharper gradients in finite volume models (reference: Moukalled, F., Mangani, L., Darwish, M., The Finite Volume Method in Computational Fluid Dynamics, 1st ed., Springer, New York, (2016), pp. 404.), and to the fact that the weakly time dependent approximation becomes less accurate as the interface movement becomes faster.

In Figures 3 and 4 below, we see the comparison between the solution to Eq.(48) and the enthalpy-porosity solutions for melting and solidification. In both cases, we see excellent agreement at low Stefan numbers, while agreement is better for melting at higher Stefan numbers. This is because the steady-state interface location is closer to zero than one, forcing the interface to move faster when solidifying as both reach steady state at approximately the same time. As faster interfaces make the weakly time dependent approximation less accurate, the greater deviation during solidification is expected.

The numerical solution accounts for the existence of the mushy zone, a region of material that is between fully molten and fully solid. Lower Stefan numbers equate to a larger mushy zone, which leads to overprediction of the interface position. This phenomenon is more present during melting due to the interpolation method used by ANSYS-Fluent to solve for liquid fraction. At higher Stefan numbers, the effect is reduced by the smaller heat of fusion values and the smoothing from numerical diffusion. From these results, we can see that the effect of the mushy zone is negligible for lower Stefan numbers, and only marginally delays reaching steady state for higher Stefan numbers.

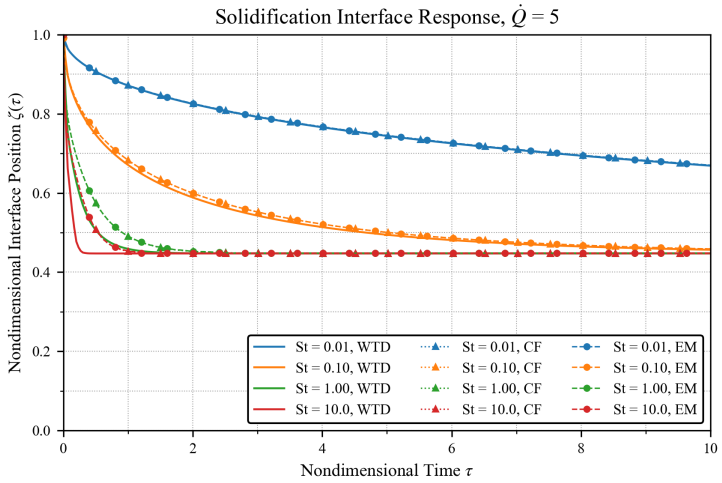

Fig. 3: Comparison between the solutions of Eq.(47) and the numerical solutions during solidification for $\dot{Q} = 5$ and various Stefan numbers

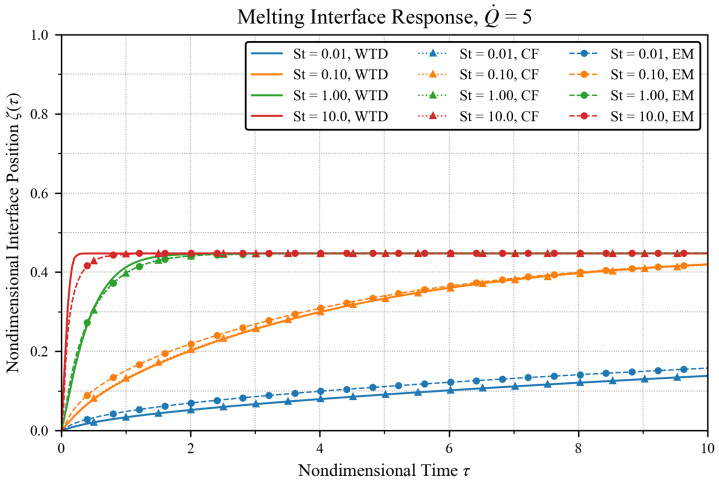

Fig. 4: Comparison between the solutions of Eq.(47) and the numerical solutions during melting for $\dot{Q} = 5$ and various Stefan numbers

The derivation in the previous section also yields the temperature profiles. Equation (26) gives the temperature profile in the liquid phase and Eq.(44) gives temperature profile in the solid phase. Figure 4 shows how the temperature distribution changes in time during solidification for $\dot{Q} = 5$ and $St = 1.0$. The dashed line at $\theta = 1$ represents the nondimensional melting temperature; above the dashed line, the material is in the liquid phase, and below, the materials is solid. We have assumed equal solidus and liquidus temperature (no mushy zone formation) in the derivation of Eq.(47), so the dashed line represents a sharp interface between the two phases. At $\tau = 0$, the red line shows that the material is completely in the liquid phase. Once the initial condition, Eq.(49) is imposed, the material begins to solidify at the outer wall and the phase change front moves inward. Note the differences in slopes between the liquid and solid phases as the front moves to steady-state. The difference in the slopes of the temperature gradients helps to drive the phase change process through equilibration. As time increases and the system approaches steady-state, the slopes of each phase at the interface approach each other and the temperature profile approaches the familiar parabolic shape, characteristic of systems with internal heat generation.

In Fig 5 we see a similar process with $\dot{Q} = 5$ and $St = 1.0$, but for melting. At $\tau = 0$, the material is completely solid and as it melts, the phase change interface moves outward until it reaches its steady-state, parabolic profile.

Two sets of profiles are presented for the numerical solutions: temperature and enthalpy. Enthalpy is a thermodynamic state variable well-suited to isothermal phase change as it expands the phase change process from an infinitesimal region to one of finite size. This allows us to see the growth and decay of the mushy zone as a function of time. Enthalpy is related to temperature by the following:

$$h = c_p T + \beta \Delta h_f \tag{51}$$

Where β is the fraction of the material in the liquid phase. Figure 5 presents the temperature and enthalpy profiles for solidification at $\dot{Q} = 5$ and $St = 1.0$. Similar to the temperature profile figures generated by the weakly time dependent approximation, the dashed line of the left figure at $\theta = 1$ represents the nondimensional melting temperature, above which the material is molten and below which the material is solid. For the righthand figure, the lower dashed line at $h = 0$ corresponds to the critical point. Below this line, $\theta < 1$ and the material is solid. The upper dashed line at $h > 1$ corresponds to the heat of fusion. Above this line, $\theta > 1$ and the material is liquid. Between these two lines, $\theta = 1$, and the material is "mushy" and contains both liquid and solid material. In solidification cases, it can be seen that the material instantaneously transitions from liquid to solid, suggesting the assumption of no mushy zone is valid.

Temperature and enthalpy profiles for the same conditions of $\dot{Q} = 5$ and $St = 1.0$ but for melting are presented in Figure 6. In the enthalpy profile we see that at low τ, a curve forms in the mushy zone before tending towards a step change from solid to liquid. This suggests that the mushy zone has greatest impact at early stages of melting, but tends towards negligible size as time advances.

5 Conclusions

An approximate solution to the Stefan problem with internal heat generation in cylindrical coordinates is derived and compared with ANSYS-Fluent enthalpy-porosity simulations. The solution method, deemed the "weakly time dependent approximation", involves the assumption that the interface moves slowly enough that the method of separation of variables is valid. Despite this stringent assumption, comparison to the numerical method of catching of the front into a space grid node shows that this approximation fails only at large Stefan numbers, and early times.

In solidification processes, the ANSYS-Fluent simulations show that there is no formation of the mushy zone, whereas melting processes produce mushy zones which rapidly shrink as time progresses. Conceptually, this shows that a sharp-interface approximation is valid for solidification processes, or relatively slow melting processes. This is further shown by the comparison between the Fluent simulations and the weakly time dependent approximate solutions. During both solidification, and melting processes, the interface position predicted by the Fluent simulation is closely matched by the approximate solution, differing only for times where the interface is moving quickly, where the weakly time dependent approximation is expected to fail.

Therefore, for slow melting, and all solidification processes it is valid to use a sharp-interface approximation. For slow processes, or long-time predictions, the weakly time dependent approximation—which greatly simplifies the analysis of this otherwise extremely complex system—Accurately follows a full simulation, including mushy zone considerations.

References

[1] Lamé, G., and Clapeyron, B., 1831. "Memoire sur la solidification par refroidissement d'un globe liquide". *Annales Chimie Physique,* **47**, pp. 250–256.

[2] Stefan, J., 1889. "Memoire sur la solidification par refroidissement d'un globe liquide". *Sitzungsberichte deer k.k. Akademie der Wissenschaften in Wien Mathematische-Naturwissenschaften,* **Abteilung II**, pp. 965–983.

Appendix A: Justification for Neglecting Free Convection

[1] [2] We can justify neglecting convection due to the lack of pumping in the liquid phase, and the assumed constant value of the thermophysical properties. Free convection can also be found to be negligible through analysis of the Nusselt number, which is the ratio of convective to conductive heat transfer. For a free convective flow this parameter can be calculated by the Elenbaas [1] formula:

$$Nu = \frac{1}{24} Ra_m \left[1 - exp\left(-\frac{35}{Ra_m} \right) \right]^{3/4} \tag{52}$$

This formula is taken from paper [2] after correcting the sign in the exponent. It is valid for free convection in vertical parallel plate configurations and can be applied to cylindrical configurations as the gravity vector would not cross two cylindrical shells sharing an origin. $Ra_m = Ra\frac{\omega}{L}$ is a modified Rayleigh number, where $\omega = D/2 * \zeta$ is a distance between the center of the rod and the melting front, D is the rod diameter, ζ is the non-dimensional coordinate of the melting front, and L is the length of the rod. The classical definition of the Rayleigh number is:

$$Ra = \frac{\rho^2 c_p \beta \Delta T \omega^3}{\mu \lambda} \tag{53}$$

Where ρ is liquid density, c_p is heat capacity, β is the volume coefficient, μ is dynamic viscosity, and λ is thermal conductivity. Since convection can only take place in the liquid phase, the temperature difference is set as the difference between the temperature at the center of the rod, and the melting temperature at the front:

$$\Delta T = T_c - T_m \tag{54}$$

Where T_c is the temperature at the center of the rod, and T_m is the melting temperature of the material. To evaluate the effect of convection, we set the real parameters of the dioxide uranium rod for Russian reactor WWER-1000 [3,4]:

$$\begin{aligned} T_0 &= 1173K \\ D &= 7.57 * 10^{-3} \\ L &= 3.35m \end{aligned} \tag{55}$$

Taking into account the melting temperature of uranium dioxide $T_m = 3173K$ [5] and using the formula for non-dimensional temperature (Eq.(5)) to solve for T_c numerically through the method of catching of the front into a space grid node (discussed below) at steady state: $T_c = 3610.5K$. The appropriate thermophysical properties for liquid uranium dioxide can be pulled from [5] for the slightly higher central temperature of $T_c = 3673K$ as the data is tabulated for increments of 100K:

$$\begin{aligned} \rho &= 8346.5 \frac{kg}{m^3} \\ c_p &= 365 \frac{J}{kgK} \\ \lambda(T = 3473K) &= 2.8 \frac{W}{mK} \\ \mu &= 3.48 * 10^{-3} Pa * s \\ \beta &= 1.112 * 10^{-4} K^{-1} \end{aligned} \tag{56}$$

Fig. 1 shows the Nusselt number as a function of front position within the rod. The temperature difference was calculated using the catching the front method with just conduction. This is valid because convection would facilitate heat transfer, and thus the temperature difference would be smaller (and therefore the Nusselt number would be smaller), thus using a model with just conduction overestimates the importance of convection. Fig.5 shows that at a steady-state regime: $\zeta \approx 0.45$(determined by the quasi-static approximation in Appendix B), $Nu \approx 0.017$. Meaning that the convective heat transfer is 1.7% the size of the conductive heat transfer. Consequently, we can neglect free convection during considerations of a melting rod.

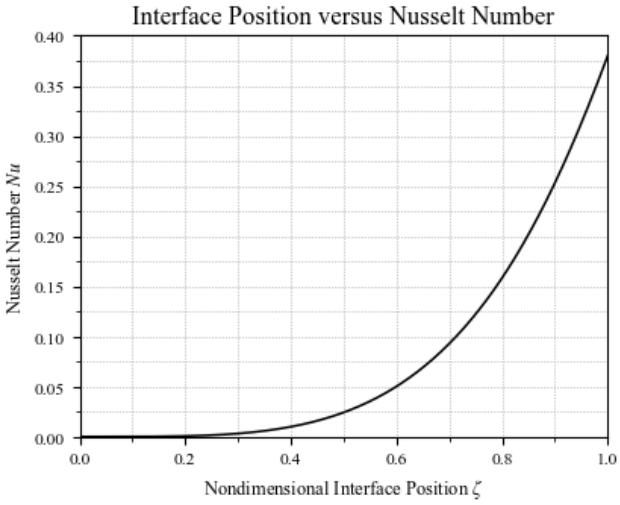

Fig. 5: Nusselt number variation during melting front movement

Appendix B: Quasi-Static Solution

The quasi-static approximation, is one in which the temperature is assumed to have negligible temporal variation. Crepeau et. al. treated the Stefan problem with internal heat generation in several geometries using this method.(Cite Approximate Solutions Paper) For the cylindrical case with constant boundary temperature the quasi steady state solutions (Eqns. (17) and (31)) were the temperature profiles used in the dimensionless interface equation Eq.(9), doing this results in

$$\frac{1}{St}\frac{d\zeta}{d\tau} = \frac{4+\dot{Q}(\zeta^2-1)}{4\zeta\ln\zeta} \tag{57}$$

Eq.(57) is especially useful for determining steady state behavior, which occurs when $\frac{d\zeta}{d\tau} = 0$, solving the resulting algebraic equation yields

$$\zeta_{ss} = \sqrt{1-\frac{4}{\dot{Q}}} \tag{58}$$

This expression gives two important results: (1) the minimum value for $\dot{Q}$ is 4, and the condition for an non-static front is $\dot{Q} \geq 4$; and (2) for the $\dot{Q}$ used in this paper ($\dot{Q} = 5$) the steady-state interface position is $\zeta_{ss} \approx 0.45$